RSC Advances

PAPER

Cite this: *RSC Adv.*, 2015, **5**, 88241

Fulleropyrrolidine molecular dumbbells act as multi-electron-acceptor triads. Spectroscopic, electrochemical, computational and morphological characterizations†

Aleksandra Mitrović,[a] Jelena Stevanović,[a] Milos Milčić,[a] Andrijana Žekić,[b] Dalibor Stanković,[c] Shigui Chen,[d] Jovica D. Badjić,[d] Dragana Milić[a] and Veselin Maslak*[a]

Received 13th August 2015
Accepted 12th October 2015

DOI: 10.1039/c5ra16309a

www.rsc.org/advances

We synthesized three dumbbell-like compounds **2a–c**, each containing two C_{60} groups at the periphery and pyromellitic diimide (PMDI) in the middle, and examined their electronic as well as assembly characteristics with both experimental and computational methods. Cyclic voltammetry (CV) measurements revealed that each of three electron-accepting (AAA) triads could accommodate up to eight electrons. Computational studies (density functional theory, DFT) of **2a–c** at PBEPBE/6-311G(d,p) level of theory, with B3LYP/6-31G(d) optimized geometries, revealed that HOMO–LUMO energy gaps are similar to those of the model compound [6,6]-phenyl-C_{61}-butyric acid methyl ester (PCBM). Compounds **2a–c** were also found to assemble into vesicles and nanoparticles on the copper grid (100–300 nm, TEM), while giving more sizeable aggregates after a deposition on the glass (SEM, >5 μm). Understanding the packing of **2a–c** on various solid substrates, as well as the assembly characteristics in general, is important for tuning the properties and fabrication of electronic/optical devices. On the basis of the results of conformational analysis (MM and DFT calculations), we deduced that different alkyl spacers in **2a–c** ought to play a role in π–π interactions between the aromatic components of the triad to guide the packing and therefore morphology of the material.

Introduction

In the pursuit of useful nano-electronic devices, scientists have incorporated electron-accepting fullerenes into a large number of hybrid structures.[1–6] These systems are often composed of C_{60} conjugated to planar aromatics to generate molecules in which individual characteristics of the components are often modulated, to give rise to new properties.[7] Platforms with one or two C_{60} groups, covalently attached to electroactive species, are labeled as fullero-dyads and fullero-triads. Importantly, different synthetic strategies have been developed for accessing architectures like C_{60}–donor (AD), C_{60}–acceptor (AA) or C_{60}–donor–C_{60} (ADA). Within these structures, the electronic and electrochemical properties of C_{60} are modulated to allow energy and/or electron transfer between the sites.[8–13] It is important to note that one of the highest power conversion efficiencies (PCE) in solution-processed organic photovoltaic cells is based on the polymer blends with fullerene derivative as the acceptor component.[14,15]

Still, fullerene-building blocks are yet to become essential components of practical electrical conductors, photovoltaic cells, electroluminescence devices and field-effect transistors.[16] It appears that the key challenge for constructing fullerene-based devices, having a desired performance, is in achieving a high level of control over the material's morphology at the nano scale.[17] In line with it, directional noncovalent forces, such as hydrogen bonding and aromatic interactions, could enable a control of the self-assembly process for creating more ordered structures to perhaps permit the bottom-up engineering of fullerene-based devices.[18–20]

In accord with the discussion, dumbbell-like molecules (Fig. 1) consisting of two π-bridged fullerenes (C_{60}–π system–C_{60}) have been of an interest to both chemists and materials scientists. Due to the presence of two spheroid units, at the periphery, these triads are expected to have an improved solubility, such enabling more extensive examination and potential application. In addition, the fullerene groups can at periphery act as "molecular alligator clips" for anchoring to give a low

[a]*Faculty of Chemistry, University of Belgrade, Studentski trg 16, P. O. B. 51, 11158 Belgrade, Serbia. E-mail: vmaslak@chem.bg.ac.rs*

[b]*Faculty of Physics, University of Belgrade, Studentski trg 12, 11000 Belgrade, Serbia*

[c]*Innovation Center of the Faculty of Chemistry, Studentski trg 12, 11000 Belgrade, Serbia*

[d]*Department of Chemistry and Biochemistry, The Ohio State University, 100 West 18th Avenue, Columbus, Ohio 43210, USA*

† Electronic supplementary information (ESI) available: Scheme S1; scanned NMR spectra of **2a–c**; Tables S1 and S2; Fig. S1–S6. See DOI: 10.1039/c5ra16309a

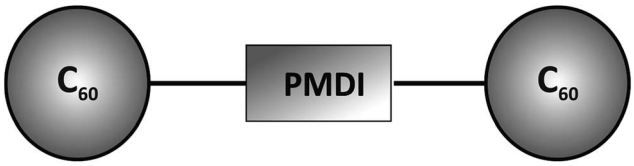

Fig. 1 Dumbbell design.

spread of low-bias conductance.[21] As examples of symmetric triads prepared recently, the following electron-donating units have been used to comprise the central core: oligomers (OPVs, OTVs, OPEs),[22–25] triphenylamines (TPhAs),[26] phenyl/fluorene,[21] dithienosilole-dibenzothiadiazole (DTSDBT),[27] tetrathiafulvalene (TTF),[28] 6*b*,10*b*-dihydrobenzo[*j*]cyclobut[*a*]acenaphthylene (DBCA).[29] Interestingly, only few systems have been made to carry an electron-accepting central unit. In one instance, Champness, Khlobystov *et al.* examined the utility of the triad having 3,4,9,10-perylene tetracarboxylic diimide (PTCDI) group bridging two fullerenes. This system, with multiple redox sites, was capable of accommodating up to six electrons in a predictable and controllable manner.[30] Naphtalenetetracarboxylic diimide (NTCDI), as another representative, have been employed to act as a component of fullerene-based rotaxanes.[27] These compounds contained two C_{60} fullerenes, acting as stoppers at both termini, while the NTCDI unit would form noncovalent contacts with the rotaxane's macrocycle.[27] In line with these efforts, we hereby describe a study of three symmetric triads **2a–c** containing two fulleropyrrolidines covalently attached to pyromellitic diimide (PMDI) *via* alkyl chains (Scheme 1). We first prepared and characterized compounds **2a–c** (C_{60}–PMDI–C_{60}, Scheme 1) and then examined their electronic, electrochemical and assembly characteristics.

Experimental section

Synthesis of materials

Compounds **2a–c** are brown solids, stable at ambient conditions. These molecules were obtained in moderate yield 42–55%, by reacting pyromellitic acid anhydride (PMAA) with fulleropyrrolidine salts **1a–c**[31] (Scheme 1). To optimize reaction conditions, we varied solvent composition CH_3CO_2H/quinoline and adjusted microwave irradiation power and time (see Table S1†). In particular, a suspension of **1a–c** (0.0052 mmol) and pyromellitic acid anhydride (0.0026 mmol) in CH_3CO_2H/quinoline = 1 : 1 mixture (1.2 mL) was irradiated in a microwave reactor for 30 min, with an inner temperature of 130 °C and applied pulse of 300 W. Crude product was precipitated by the addition of methanol and then purified by column chromatography (SiO_2) with $CH_3CO_2CH_2CH_3$/toluene = 1/9 mixture as an eluent. Subsequent precipitation with methanol, from a highly concentrated solution in $CHCl_3$, gave pure **2a–c** as brown powders in 42–55% yields.

Compound 2a. Yield 2.5 mg (55%). IR (ATR) $\tilde{\nu}$: 2930, 1719, 1370, 1093, 760, 481 cm^{-1}. UV-VIS ($CHCl_3$) λ (ε, M^{-1} cm^{-1}): 430 (4200), 704 (380). ^1H ($CDCl_3$, 500 MHz) δ 8.37 (s, 4H), 4.48 (s, 8H), 4.47 (s, 4H), 4.34–4.28 (m, 4H), 3.50–3.44 (m, 4H). ^{13}C ($CDCl_3$, 125 MHz) δ 166.2 (4C); 154.8 (Cf-12); 147.5 (Cf-17); 146.4 (Cf-7); 146.1 (Cf-11); 145.6 (Cf-16); 145.5 (Cf-5); 144.7 (Cf-9); 143.3 (Cf-15); 142.8 (Cf-8); 142.2 (Cf-6); 142.1 (Cf-14); 142.0 (Cf-4); 141.8 (Cf-12,13); 141.1 (Cf-10); 140.3 (Cf-3); 138.8 (4C), 136.2 (4C); 118.9 (2CH); 70.8 (4C); 67.5 ($4CH_2$); 37.5 ($2CH_2$); 33.8 ($2CH_2$). MALDI/TOF: *m*/*z* calcd for $[C_{138}H_{18}N_4O_4+H]^+$ 1796, measured 1796.

Compound 2b. Yield 2.0 mg (42%). IR (ATR) $\tilde{\nu}$: 2925, 1719, 1368, 1118, 728, 526 cm^{-1}. UV-VIS ($CHCl_3$) λ (ε, M^{-1} cm^{-1}): 430 (5200), 704 (380). ^1H ($CDCl_3$, 500 MHz) δ 8.24 (s, 4H); 4.36 (s, 8H); 3.94 (t, 4H, J = 6.5); 3.13 (t, 4H, J = 7.5); 2.12–2.07 (m, 4H); 1.99–1.94 (m, 4H). ^{13}C ($CDCl_3$, 125 MHz): δ 165.6 (4C); 154.5 (Cf-12); 147.0 (Cf-17); 146.0 (Cf-7); 145.8 (Cf-11); 145.7 (Cf-16); 145.4 (Cf-5); 145.2 (Cf-9); 145.0 (Cf-15); 144.3 (Cf-8); 142.9 (Cf-6); 142.4 (Cf-14); 142.0 (Cf-4); 141.8 (Cf-12,13); 141.7 (Cf-10); 140.0 (Cf-3); 137.0 (4C); 136.0 (4C); 118.0 (2CH); 70.3 (4C); 67.7 ($4CH_2$); 53.8 ($2CH_2$); 38.3 ($2CH_2$); 26.4 ($2CH_2$); 26.1 ($2CH_2$). MALDI/TOF: *m*/*z* calcd for $[C_{142}H_{26}N_4O_4+H]^+$ 1853, measured 1853.

Compound 2c. Yield 2.1 mg (43%). IR (ATR) $\tilde{\nu}$: 2933, 1721, 1365, 1118, 731, 525 cm^{-1}. UV-VIS ($CHCl_3$) λ (ε, M^{-1} cm^{-1}): 430 (6600), 704 (380). ^1H ($CDCl_3$, 500 MHz) δ 8.21 (s, 4H); 4.37 (s, 8H); 3.79 (t, 4H, J = 7); 3.07 (t, 4H, J = 7.5); 1.96–1.90 (m, 4H); 1.86–1.79 (m, 4H); 1.74–1.68 (m, 4H); 1.58–1.52 (m, 4H). ^{13}C ($CDCl_3$, 125 MHz) δ 165.6 (4C); 154.7 (Cf-12); 147.0 (Cf-17); 146.0 (Cf-7); 145.8 (Cf-11); 145.8 (Cf-16); 145.4 (Cf-5); 145.2 (Cf-9); 145.0 (Cf-15); 144.3 (Cf-8); 142.9 (Cf-6); 142.4 (Cf-14); 142.0 (Cf-4); 141.8 (Cf-12,13); 141.7 (Cf-10); 140.0 (Cf-3); 137.0 (4C); 136.0 (4C); 117.8 (2CH); 70.4 (4C); 67.7 ($4CH_2$); 54.6 ($2CH_2$); 38.4 ($2CH_2$); 28.7 ($2CH_2$); 28.5 ($2CH_2$); 27.1 ($2CH_2$); 26.8 ($2CH_2$). MALDI/TOF: *m*/*z* calcd for $[C_{146}H_{34}N_4O_4+H]^+$ 1909, measured 1909.

Computational details

In order to investigate π–π aromatic interactions between fullerene and PMDI moieties, we employed DFT calculations. It

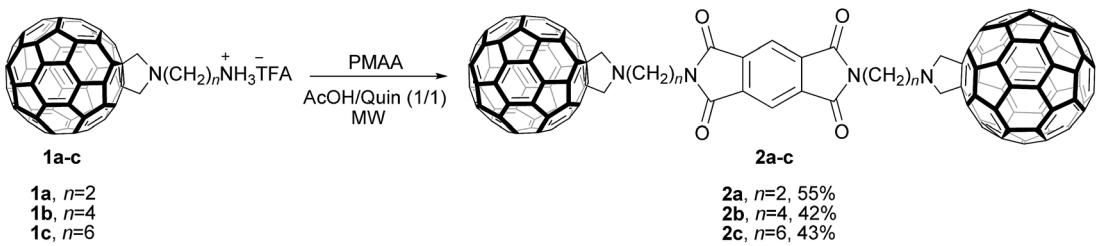

Scheme 1 Synthesis of C_{60}–PMDI–C_{60} molecular dumbbells **2a–c**.

was shown previously[32] that B97-D functional,[33] with included Grimme's D2 dispersion correction, is the method of choice for computing π–π stacking interactions. This method was successfully applied for quantifying concave–convex interactions in corannulene[34] and coronene[35] dimers, fullerene interactions with corannulenes and sumanenes[36] and fullerene interactions with molecular tweezers.[37,38] The geometry of fullerene–PMDI complex was fully optimized with B97-D functional using triple zeta basis set (TZVP) from Ahlrichs and coworkers.[39] Interaction energy (E_{int}) was calculated at the same level of theory (B97-D/TZVP) with included Boys and Bernardi counterpoise correction[40] to account for basis set superposition error (BSSE). Deformation energy (E_{def}) was calculated as a difference between the energy of monomers in their optimal geometries and their geometries within the complex. The full complexation energy ($E_{complex}$) was obtained using the formula:

$$E_{complex} = E_{int} - E_{def} \quad (1)$$

Due to the large size and conformational flexibility of **2a–c**, detailed computational study was performed only on compound **2a** containing two CH_2 groups. The conformational search was performed with molecular mechanic force field implemented in AMMP program, using systematic search method with Vega ZZ (version 3.0) interface.[41] The geometries of three most abundant conformers of compound **2a** were fully optimized in gas phase with B3LYP functional and 6-31G(d) basis set with included Grimme's D2 dispersion correction. Energies of the conformers were calculated on B3LYP/6-31G(d) optimized geometries using same functional and dispersion correction, but with larger 6-311G(d,p) basis set in toluene solution. Solvent effect was simulated with SMD implicit solvation method.[42] Non-Covalent Interactions (NCI) visualization index is calculated using NCI plot program.[43] HOMO and LUMO orbital energies are calculated in gas phase, on B3LYP/6-31G(d) optimized geometries, using PBEPBE functional and relatively large basis set 6-311G(d,p). This method was recently proven to be quite reliable in calculating HOMO–LUMO energies and other molecular properties in fulleropyrrolidine[44] and PCBM-like fullerene derivatives.[45]

Properties of the first excited state were investigated using TD-DFT technique, with B3LYP functional and 6-311G(d,p) basis set. The Fukui function and spin densities were calculated with B3LYP/6-311G(d,p) method by adding electron to B3LYP/6-31G(d) optimized geometries. All the orbitals were drown in gOpenMol[46] program from HF/6-311G(d,p) wavefunction.

All the quantum chemical calculations were done in Gaussian 09 program package.[47]

Results and discussion

Optical properties

UV-vis spectra of **2a–c**, dissolved in $CHCl_3$, were recorded between 300 and 800 nm at a room temperature (Fig. 2). Optical absorptions are for all three compounds identical, with bands characteristic for fulleropyrrolidine derivatives. The UV region of **2a–c** is dominated by the strong absorption, which

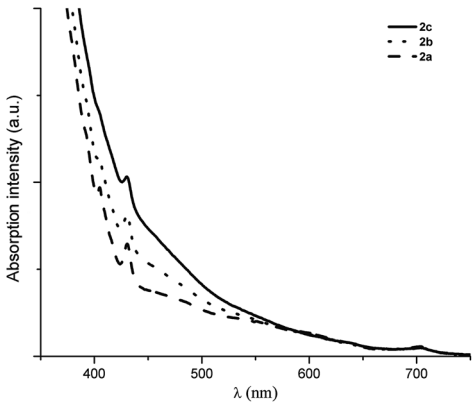

Fig. 2 UV-vis spectra of compounds **2a–c**.

corresponds to the electronic transitions with high oscillator strength from the ground state to the excited states (0 → *0), analogously to the parent C_{60}. In the visible region, a shoulder at 430 nm is accompanied with a weak band around 700 nm. The signal at 430 nm indicates the presence of [6,6]-functionalized fullerene derivatives.[48]

The UV-vis spectra of **2a–c** appear to be a superposition of those corresponding to fulleropyrrolidine and PMDI components. The emission spectra of **2a–c** (400–850 nm, Fig. S1†) were collected after excitation at 400 nm and are in good agreement with the absorption features. The *0 → 0 emission (λ_{max}, 709 nm) and 0 → *0 absorption bands (λ_{max}, 704 nm) differ very slightly to provide additional evidence for the absence of a charge transfer interaction between two chromophores.

Electrochemistry

The electrochemical characteristics of fullerene-based **2a–c** were investigated with cyclic voltammetry in *o*-dichlorobenzene–DMF = 2 : 1 solution mixture (Fig. 3). In order to understand the electron transfer pathways, CV data were collected for structurally similar reference compounds *N*,*N*-dihexylpyromellitic diimide (**DHPMDI**) and *N*-methylfulleropyrrolidine (**NMFP**).

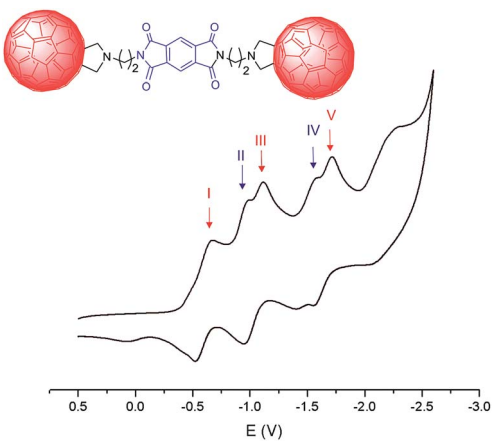

Fig. 3 Cyclic voltammogram (CV) of **2a** at 50 mV s^{-1} rate in *o*-dichlorobenzene : DMF = 2 : 1 mixture, containing 0.1 M nBu_4NPF_6.

The half-wave potential values for all compounds are given in Table 1. In the potential range between 0 and −2.8 V five quasi-reversible reductions were observed for **2a** and **2b**, whereas **2c** showed four reduction waves. For illustrative clarity, CV curves for **2b–c** and reference compounds are omitted from Fig. 3 and can be found in Fig. S2.† As can be seen from Table 1, the half-wave potential values, associated with the first fullerene reduction, are cathodically shifted by 100–120 mV, compared to the parent C_{60}. Indeed, a decrease in the electron activity of the functionalized fullerene is expected due to a partial loss in π-conjugation.[49] In the second reduction process, one electron is accepted by the PMDI moiety: the half wave potential of −1.16 V for **2a** (−1.13 V for **2b**, −1.15 V for **2c**) compared with DHPMDI (1.10 V) indicates the increase of electronic density on this electron-poor organic addend. Third $E_{1/2}$ value can be assigned to fullerene cages due to its good correlation with second reduction peak of the model NMFP (−1.28 V, Table 1). As the reduction goes to more negative potentials, the assignment of the redox processes, based on a similarity to the corresponding model compounds, becomes less straightforward. We assign reduction peaks IV and V, to the second PMDI and third C_{60} reduction, respectively. For compound **2c**, the last two reduction peaks could not be resolved by changing the scan rate of the experiment. A gradual broadening of the redox waves might be ascribed to the presence of longer and more flexible alkyl chains (six CH_2 groups) causing a decrease in the rate constant characterizing electron transfer processes at the electrode surface.

In line with reductions of other related symmetric C_{60}-dimers and triads,[30,50] each of the fullerene reduction waves is in **2a–c** commensurate with a two-electron uptake. The peak current of these reductions is thus higher than for those associated with the PMDI reductions, indicating that the latter correspond to a one-electron uptake.

Cyclic voltammograms of all three triads (Fig. S2†) show that C_{60} and PMDI moieties are accommodating electrons independently of each other. It should also be noted that no significant influence of the alkyl spacer on the electrochemical properties was found, except for the dumbbell **2c** where a greater conformational flexibility of alkyl chains, perhaps, causes a poor resolution of the reduction peaks. As shown in Table 2, dumbbell-like **2a–c** display a substantial electrochemical response with the ability of accommodating up to eight electrons to emphasize its possible use as an PCBM-like electron acceptor in polymer solar cells.

Table 1 Cyclic voltammetry data (half-wave potentials)

Compd	Potentials *vs.* Fc/Fc^+ (V)					
C_{60}	−0.69	−1.18	—	−1.69	—	−2.28
2a	−0.81	−1.16	−1.27	−1.69	−1.86	
2b	−0.81	−1.13	−1.22	−1.74	−1.83	
2c	−0.79	−1.15	−1.27	—	−1.86[a]	
NMFP	−0.81	—	−1.28	−1.72	−1.92	
DHPMDI	—	−1.10	—	−1.81	—	

[a] Broad peak.

Table 2 Comparison of HOMO energy, LUMO energy, and HOMO–LUMO energy gap of C_{60}, PCBM and conformers of **2a**

Compd	Parameters	PBEPBE/6-311G(d,p)[a]
C_{60}	HOMO/eV	−5.867
	LUMO/eV	−4.181
	E_{gap}/eV	1.686
PCBM	HOMO/eV	−5.522
	LUMO/eV	−4.006
	E_{gap}/eV	1.516
2a	HOMO/eV	−5.575[b], −5.447[c], −5.417[d]
	LUMO/eV	−4.234[b], −4.238[c], −4.257[d]
	E_{gap}/eV	1.341[b], 1.209[c], 1.16[d]

[a] Cited from ref. 44. [b] Extended conformer. [c] Single-folded conformer. [d] Double-folded conformer.

DFT calculations

The Wudl group has extensively studied electronic properties of spiromethanofullerene with fluorenyl planar framework being perpendicular to the surface of C_{60}.[51,52] They concluded that this topological arrangement is responsible for 'though-space' interactions between fluorenyl moiety and C_{60} causing the first reduction potential to become less negative than the same one in parent C_{60}. This prompted us to investigate possible concave/convex π–π aromatic interactions between electron accepting organic addends (C_{60} and PMDI) within **2a–c** and to study whether their spatial arrangement has a measurable effect on the electronic and self-assembly properties of these compounds.

A π–π aromatic interaction between fullerene and PMDI (as a model complex) were investigated computationally with B97-D/TZVP method. In the optimized geometry of fullerene–PMDI complex (Fig. 4a) a PMDI molecule has adopted a concave geometry with 8.0° deviation from planarity. This bending of the PMDI molecule allows a greater contact surface between molecules which could give rise to stronger π–π interactions.[35] The calculated complexation energy ($E_{complex}$) is 9.76 kcal mol^{-1}. This complexation energy is relatively small and only half the size of the complexation energy of fullerene with corannulene (17.03 kcal mol^{-1}) and sumanene (18.47 kcal mol^{-1}) aromatics, both well known as concave hosts for fullerene.

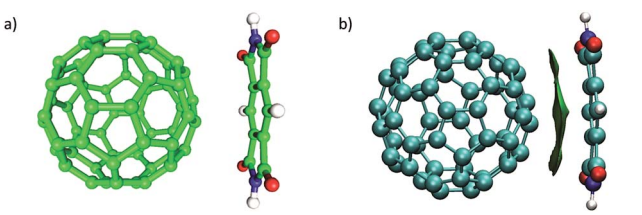

Fig. 4 (a) Optimized geometry of fullerene–PMDI complex. (b) NCI visualization index of fullerene–PMDI complex. Green surface indicates the area of weak, attractive π–π interactions between two molecules.

Despite, the obtained values indicate a possibility for non-covalent intermolecular interactions in compounds **2a–c**, especially in polar non-aromatic solvents.

The nature of the interaction was further investigated using non-covalent interactions (NCI) visualization index.[46] The NCI index, calculated for the fullerene–PMDI complex (Fig. 4b), reveals a large area of weak and attractive π–π contacts as a primary source of the interaction between these two molecules.

Conformational search for stable conformers of compound **2a** produced three clusters of conformers (Fig. 5). In the first cluster (Fig. 5a) were the structures with both fullerene alkyl arms fully extended away from the PMDI part with no intramolecular π–π contacts. In the conformers of the second cluster (Fig. 5c), one fullerene arm is folded toward the PMDI part and in the third cluster both fullerene arms are folded towards PMDI part of the molecules (Fig. 5b). One representative structure of each cluster was additionally optimized and structures of extended, single-folded and double-folded conformers were obtained (Fig. 5a–c). The potential energies of all three conformers of compound **2a** in toluene solution are evaluated at B3LYP/6-311G(d,p) level of theory. The most stabile conformation is single-folded (Fig. 5c), while double-folded (Fig. 5b) and extended (Fig. 5a) conformations are somewhat less stable (1.1 kcal mol^{-1} and 4.1 kcal mol^{-1}, respectively).

It is worth noting that entropic factors are not included in our analysis. The entropy could, perhaps, significantly contribute to the stability of conformers, and especially in the solvent phase.

The second part of our computational investigation was focused on understanding the electronic properties of compound **2a**. HOMO–LUMO energy gaps were calculated for the extended, single-folded (Fig. 5b) and double-folded (Fig. 5c) conformers. Obtained results were compared to the appropriate values for the reference C_{60} and PCBM. Summarized data are shown in Table 2. It can be seen that HOMO–LUMO energy gap is 0.34–0.52 eV lower for all conformers of compound **2a** when compared to C_{60}. Concurrently, both HOMO (0.29–0.45 eV) and LUMO energies (0.08–0.05 eV) are more negative for three conformers of **2a**. On the other hand HOMO/LUMO energies and E_{gap} of all **2a** conformers more closely reassemble those of the PCBM acceptor (Table 2). All conformers of **2a** display higher-lying LUMO and reduced bandgap which is very important in terms of improving the open-circuit voltage V_{oc} and light harvesting capacity of the acceptor component in BHJ solar cells.[53] Our further investigation of electron accepting features of compound **2a** was oriented towards calculating the properties of excited state. TD-DFT calculations at B3LYP/6-311G(d,p) level of theory was employed in order to investigate the properties of first excited state. TD-DFT calculations predicts that first energy transitions will occur at energies of 1.881, 1.860 and 1.873 eV for extended, single folded and double folded conformer, respectively. The electron density difference maps between first excited and ground state are shown in Fig. 6. For the extended and single folded conformation there is no charge transfer between fullerene and PMDI parts of the molecule, indicating attenuated potential for the OPV n-phase material; excitation is localized on the fullerene cage (Fig. 6a and b). Due to favorable overlap of orbitals, a little of the electron transfer from fullerene to PMDI is observed in the double folded conformation (Fig. 6c).

Similarly, the Fukui function and Mulliken spin densities calculations (see ESI Fig. S3 and S4†) have shown that fullerene cage will be the most probable target of nucleophile attack. For radical monoanionic form of compound **2a**, from 75% to 90% of additional electron spin density is located at the two fullerene cages.

Morphology characterization

The aggregation behavior of compounds **2a–c** was investigated with scanning electron microscopy (SEM) and transmission electron microscopy (TEM). Samples were prepared by drop-drying process, akin to earlier procedures used in studying the assembly of C_{60}.[54] The aggregation of fullerene derivatives has proven to be an efficient approach toward creating remarkable architectures like: 1D fibers, 2D sheets, 3D spheres and flower-like objects.[18,55–59] These interesting structures exist as a direct consequence of the three-dimensional shape of C_{60} undergoing aromatic interactions. In addition, different functional groups at the surface of fullerenes and the choice of solvents determine the final outcome of self-assembly process.

To investigate the effect of the medium polarity on the aggregation of **2a–c**, we used the following solvents: toluene, *o*-dichlorobenzene (ODCB) and chloroform as well as their 2 : 1 mixtures with 1,4-dioxane and iso-propanol. All samples were

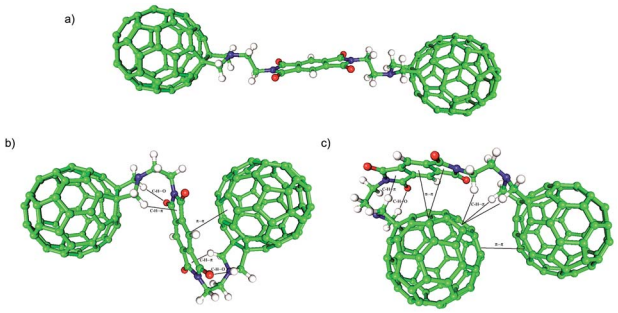

Fig. 5 Mapping non-covalent intermolecular interactions in **2a**.

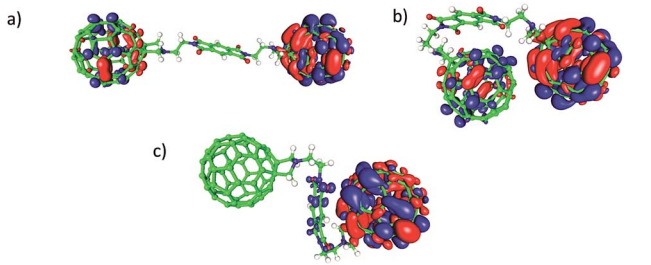

Fig. 6 Electron density difference maps between first excited and ground state for (a) extended, (b) single folded and (c) double folded conformer of compound **1a**. The blue lobes represent area of higher electron densities in excited state than in the ground state. The red lobes represent area of lower electron densities in excited state than in the ground state.

prepared in the following manner prior to SEM/TEM imaging. Compounds **2a–c** were dissolved (1 mg) in 1 mL of solvent (~0.5 μM) and a drop of the solution was deposited onto a glass-plate (SEM). Under toluene atmosphere, the solvent was allowed to evaporate during 48 h at a room temperature (SEM). For TEM measurement, 0.25 mM solution of **2a–c** was deposited on a copper grid and subjected to drying under ambient conditions.

Different modes of assembly of **2a–c** were observed by SEM and TEM measurements (Fig. 7 and 8). The apparent discrepancy resulted from different conditions used in the preparation of samples. The aggregation of molecules ought to be a function of the solid substrates on which it took place, the concentration of molecules and drying conditions (time, temperature, *etc.*). Compound **2a** assembled into nanoparticles (Fig. 7a), while **2b** and **2c** (only **2c** shown in Fig. 7b) showed a tendency to form unilamellar vesicles. The sizes of the vesicles were generally uniform with 200–300 nm in diameter. By a closer inspection of the single vesicle (HR TEM) we estimated the thickness of its membrane to be 4.4 nm. The width corresponds well to the length of the extended conformer of **2c** (Fig. 7c). As presented in Fig. 8, compound **2a** dissolved in toluene/dioxane (2 : 1) assembles into fiber containing sheets (or bundles) while in the same solvent mixture **2b** aggregates into smaller hank-like objects (Fig. 8c). When processed from toluene/^{i}Pr-OH (2/1) **2a** exhibits a flower-like structure (Fig. 8b), whereas **2b** assembles into sheet fibers (Fig. 8d).

When dissolved in $CHCl_3$/^{i}Pr-OH (2 : 1) mixture compound **2c** gave micron-size clusters (Fig. 8e), whereas in $CHCl_3$/dioxane (2/1) mixture "necklace-like" chains (Fig. 8f). In other solvent combinations compounds **2a–c** showed various self-organized architectures with the corresponding images presented in ESI (Fig. S5†).

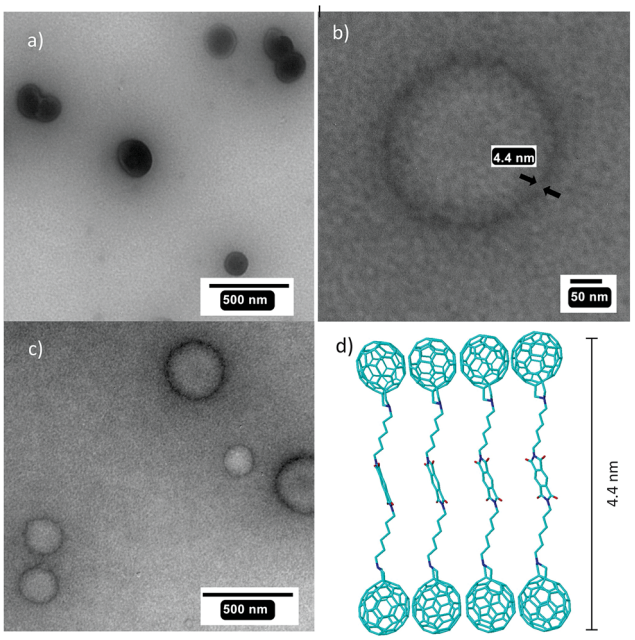

Fig. 7 TEM images of (a) **2a** and (c) **2c** (~0.25 mM) dissolved in toluene/dioxane (2 : 1) and deposited on a copper grid without staining with uranyl acetate (b) diameter of the vesicle **2c**, (d) calculated length of the extended conformer of **2c**. The thickness of the vesicular membrane is estimated to be 3 nm corresponding to the calculated length of the extended conformer of **2c**.

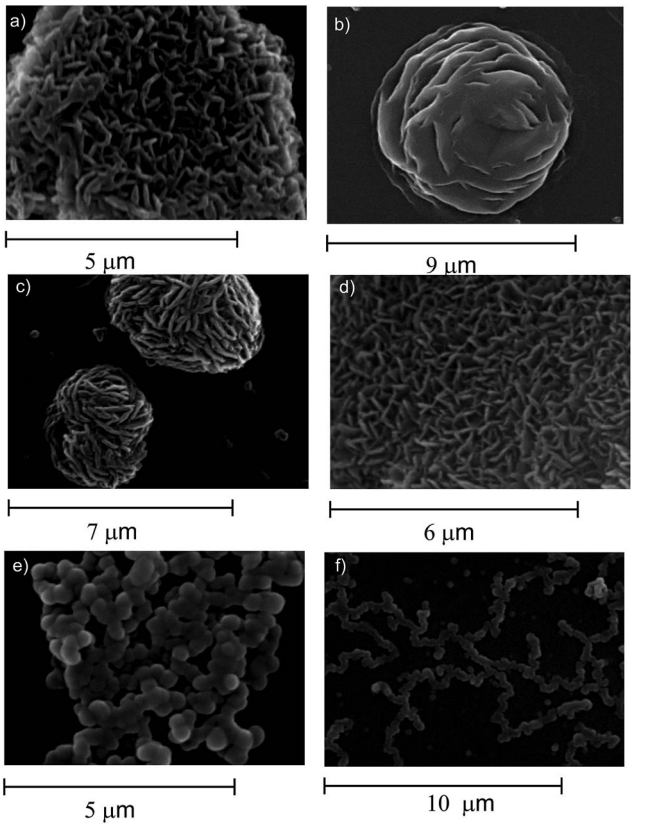

Fig. 8 SEM images of **2a** prepared from (a) toluene/dioxane, (b) toluene/^{i}Pr-OH; **2b** prepared from (c) toluene/dioxane, (d) toluene/^{i}Pr-OH and **2c** prepared from (e) $CHCl_3$/^{i}Pr-OH, (f) $CHCl_3$/dioxane.

To summarize, compounds **2a–c** have a tendency to organize into nano- and micro-sized structures as a function of the length of their alkyl chains and experimental conditions. Importantly, the length of the extended conformer **2c** bearing a hexyl chain is consistent with the thickness of the vesicle wall. This implies that the monolayer structure is in vesicles held by π–π (C_{60}/C_{60}, PMDI/PMDI) and van der Waals (CH_2/CH_2) interactions. With a large number of C_{60} exposed on the vesicle surface, "active cites" are created for fullerene–fullerene attraction between different vesicles, which could play a role in the observed hierarchical assembly by SEM.

We presume that compounds **2a** and **2b**, having shorter alkyl chains, give rise to weaker noncovalent contacts with a smaller solvophobic bias to lead to the formation of different structures, indicating a way for controlling the ordering of this type of supramolecular soft material.

Conclusions

In conclusion, we have successfully synthesized a series of fulleropyrrolidine molecular dumbbells (**2a–c**). Their electronic,

electrochemical and self-assembly characteristics were determined with UV-vis/emission spectroscopies, cyclic voltammetry, DFT calculation, scanning electron and transmission electron microscopies. CV measurements confirmed that the functionalization of C_{60} preserved its electron-accepting characteristics. Reduction potentials are in line with values measured for the model NMFP compound, and therefore consistent with the notion that there is only a weak electronic coupling between the triad units. DFT calculations suggested that these weak interactions consist of concave/convex π–π contacts between C_{60} moieties and PMDI. Different modes of supramolecular assembly were observed for **2a–c**. On the copper surface, compound **2a** with a shorter alkyl chain connecting its building units assembled into nanoparticles (**2a**). Compounds **2b** and **2c**, with longer alkyl groups, formed nanosized vesicles. On a glass surface, however, **2a–c** gave rise to larger (microsized) aggregates *via*, perhaps, a hierarchical ordering of nanoparticles and vesicles. The formation of supramolecular architectures appeared to be less dependent on the choice of the solvent and more influenced by the molecular design and the nature of supporting substrate yet other factors could also play a role. Our groups are currently examining the electronic and assembly characteristics of C_{60}/PMDI triads containing stiffer and electron conjugated/non-conjugated linking groups on which we plan to report in future.

Acknowledgements

Financial support of the Ministry of Education, Science and Technological Development of the Republic of Serbia is acknowledged (Project No. 172002). An experimental portion of this work (TEM measurements) was financially supported with funds obtained from the U.S. National Science Foundation (CHE-1305179) to JDB.

Notes and references

1 J. Roncali, *Chem. Soc. Rev.*, 2005, **34**, 483–495.
2 T. Nishizawa, K. Tajima and K. Hashimoto, *J. Mater. Chem.*, 2007, **17**, 2440–2445.
3 Y. Shirai, J.-F. Morin, T. Sasaki, J. M. Guerrero and J. M. Tour, *Chem. Soc. Rev.*, 2006, **35**, 1043–1055.
4 K. Prassides, M. Keshavarz-K, J. C. Hummelen, W. Andreoni, P. Giannozzi, E. Beer, C. Bellavia, L. Cristofolini, R. Gonzalez, A. Lappas, Y. Murata, M. Malecki, V. I. Srdanov and F. Wudl, *Science*, 1996, **271**, 1833.
5 S. Yoshimoto, E. Tsutsumi, R. Narita, Y. Murata, M. Murata, K. Fujiwara, K. Komatsu, O. Ito and K. Itaya, *J. Am. Chem. Soc.*, 2007, **129**, 4366.
6 A. Mateo-Alonso, D. M. Guldi, F. Paolucci and M. Prato, *Angew. Chem., Int. Ed.*, 2007, **46**, 8120–8126.
7 G. Mehtaa and V. Singh, *Chem. Soc. Rev.*, 2002, **31**, 324–334.
8 N. Martın, L. Sanchez, M. A. Herranz and D. M. Guldi, *J. Phys. Chem. A*, 2000, **104**, 4648–4657.
9 A. S. Konev, A. F. Khlebnikov, T. G. Nikiforova, A. A. Virtsev and H. Frauendorf, *J. Org. Chem.*, 2013, **78**, 2542–2552.
10 J. Baffreau, S. Leroy-Lhez, N. van Anh, R. M. Williams and P. Hudhomme, *Chem.–Eur. J.*, 2008, **14**, 4974–4992.
11 J. Baffreau, L. Ordronneau, S. Leroy-Lhez and P. Hudhomme, *J. Org. Chem.*, 2008, **73**, 6142–6147.
12 J. L. Segura and N. Martín, *Chem. Soc. Rev.*, 2000, **29**, 13–25.
13 N. Martın, L. Sanchez, B. Illescas and I. Perez, *Chem. Rev.*, 1998, **98**, 2527–2547.
14 K. L. J. Y. KIm, N. E. Coates, D. Moses, T. Q. Nguyen, M. Dante and A. J. Heeger, *Science*, 2007, **317**, 222.
15 G. Li, V. Shrotriya, J. S. Huang, Y. Yao, T. Moriarty, K. Emery and Y. Yang, *Nat. Mater.*, 2005, **4**, 864.
16 D. M. Guldi, B. M. Illescas, C. M. Atienza, M. Wielopolskia and N. Martın, *Chem. Soc. Rev.*, 2009, **38**, 1587–1597.
17 S. Santhosh, B. H. Mohwald and T. Nakanishi, *Chem. Soc. Rev.*, 2010, **39**, 4021–4035.
18 T. Nakanishi, *Chem. Commun.*, 2010, **46**, 3425–3436.
19 D. M. Guldi and N. Martın, *J. Mater. Chem.*, 2002, **12**, 1978–1992.
20 T. Wang, A. J. Pearson and D. G. Lidzey, *J. Mater. Chem. C*, 2013, **1**, 7266–7293.
21 J. K. Sørensen, J. Fock, A. H. Pedersen, A. B. Petersen, K. Jennum, K. Bechgaard, K. Kilsa, V. Geskin, J. Cornil, T. Bjørnholm and M. B. Nielsen, *J. Org. Chem.*, 2011, **76**, 245–263.
22 M. J. Gomez-Escalonilla, F. Langa, J.-M. Rueff, L. Oswald and J.-F. Nierengarten, *Tetrahedron Lett.*, 2002, **43**, 7507–7511.
23 N. Zhou and Y. Zhao, *J. Org. Chem.*, 2010, **75**, 1499.
24 C. Atienza, B. Insuasty, C. Seoane, N. Martın, J. Ramey, G. M. A. Rahman and D. M. Guldi, *J. Mater. Chem.*, 2005, **15**, 124–132.
25 K. Komatsu, N. Takimoto, Y. Murata, T. S. M. Wan and T. Wong, *Tetrahedron Lett.*, 1996, **37**, 6153–6156.
26 R. Zalesny, O. Loboda, K. Iliopoulos, G. Chatzikyriakos, S. Couris, G. Rotas, N. Tagmatarchis, A. Avramopoulos and M. Papadopoulos, *Phys. Chem. Chem. Phys.*, 2010, **12**, 373–381.
27 Y. Nakamura, S. Minami, K. Iizuka and J. Nishimura, *Angew. Chem., Int. Ed.*, 2003, **42**, 3158–3162.
28 J. L. Segura, E. M. Priego, N. Martın, C. Luo and D. M. Guldi, *Org. Lett.*, 2000, **2**, 4021–4024.
29 A. Sastre-Santos, C. Parejo, L. Martın-Gomis, K. Ohkubo, F. Fernandez-Lazaro and S. Fukuzumi, *J. Mater. Chem.*, 2011, **21**, 1509–1515.
30 T. W. Chamberlain, E. S. Davies, A. N. Khlobystov and N. R. Champness, *Chem.–Eur. J.*, 2011, **17**, 3759–3767.
31 A. Mitrovic, N. Todorovic, A. Zekic, D. Stankovic, D. Milic and V. Maslak, *Eur. J. Org. Chem.*, 2013, 2188–2193.
32 D. Josa, J. Rodríguez-Otero, E. M. Cabaleiro-Lago and M. Rellán-Piñeiro, *Chem. Phys. Lett.*, 2013, **557**, 170–175.
33 S. Grimme, *J. Comput. Chem.*, 2006, **27**, 1787–1799.
34 T. Janowski, P. Pulay, A. A. S. Karunarathna, A. Sygula and S. Saebø, *Chem. Phys. Lett.*, 2011, **512**, 155–160.
35 M. R. Kennedy, L. A. Burns and C. D. Sherrill, *J. Phys. Chem. A*, 2012, **116**, 11920–11926.
36 D. Josa, J. Rodrıguez-Otero, E. M. Cabaleiro-Lago, L. A. Santos and T. C. Ramalho, *J. Phys. Chem. A*, 2014, **118**, 9521–9528.

37 C. Muck-Lichtenfeld, S. Grimme, L. Kobrynb and A. Sygula, *Phys. Chem. Chem. Phys.*, 2010, **12**, 7091–7097.
38 D. Josa, J. Rodrıguez-Otero and E. M. Cabaleiro-Lago, *Phys. Chem. Chem. Phys.*, 2015, **17**, 13206.
39 A. Schafer, C. Huberund and R. Ahlrichs, *J. Chem. Phys.*, 1994, **100**, 5829–5835.
40 S. F. Boys and F. Bernardi, *Mol. Phys.*, 1970, **19**, 553–566.
41 A. Pedretti, L. Villa and G. Vistoli, *J. Comput.-Aided Mol. Des.*, 2004, **18**, 167–173.
42 A. V. Marenich, C. J. Cramer and D. G. Truhlar, *J. Phys. Chem. B*, 2009, **113**, 6378–6396.
43 E. R. Johnson, S. Keinan, P. Mori-Sánchez, J. Contreras-García, A. J. Cohen and W. Yang, *J. Am. Chem. Soc.*, 2010, **132**, 6498–6506.
44 X. Zhang, X. D. Li, L. X. Maa and B. Zhanga, *RSC Adv.*, 2014, **4**, 60342–60348.
45 H. Wang, Y. He, Y. Li and H. Su, *J. Phys. Chem. A*, 2012, **116**, 255–262.
46 L. Laaksonen, *J. Mol. Graphics*, 1992, **10**, 33–34.
47 G. W. T. M. J. Frisch, H. B. Schlegel, G. E. Scuseria, M. A. Robb, J. R. Cheeseman, G. Scalmani, V. Barone, B. Mennucci, G. A. Petersson, H. Nakatsuji, M. Caricato, X. Li, H. P. Hratchian, A. F. Izmaylov, J. Bloino, G. Zheng, J. L. Sonnenberg, M. Hada, M. Ehara, K. Toyota, R. Fukuda, J. Hasegawa, M. Ishida, T. Nakajima, Y. Honda, O. Kitao, H. Nakai, T. Vreven, J. A. Montgomery Jr, J. E. Peralta, F. Ogliaro, M. Bearpark, J. J. Heyd, E. Brothers, K. N. Kudin, V. N. Staroverov, T. Keith, R. Kobayashi, J. Normand, K. Raghavachari, A. Rendell, J. C. Burant, S. S. Iyengar, J. Tomasi, M. Cossi, N. Rega, J. M. Millam, M. Klene, J. E. Knox, J. B. Cross, V. Bakken, C. Adamo, J. Jaramillo, R. Gomperts, R. E. Stratmann, O. Yazyev, A. J. Austin, R. Cammi, C. Pomelli, J. W. Ochterski, R. L. Martin, K. Morokuma, V. G. Zakrzewski, G. A. Voth, P. Salvador, J. J. Dannenberg, S. Dapprich, A. D. Daniels, O. Farkas, J. B. Foresman, J. V. Ortiz, J. Cioslowski, and D. J. Fox, *Gaussian 09, Revision D.01*, Gaussian, Inc., Wallingford CT, 2013.
48 M. Prato and D. M. Guldi, *Acc. Chem. Res.*, 2000, **33**, 695–703.
49 T. Suzuki, Y. Maruyama, T. Akasaba, W. Ando, K. Kobayashi and S. Nagase, *J. Am. Chem. Soc.*, 1994, **116**, 1359–1363.
50 P. Timmerman, L. E. Witschel, F. Diederich, C. Boudon, J.-P. Gisselbrecht and M. Gross, *Helv. Chim. Acta*, 1996, **79**, 6–20.
51 M. Eiermann, R. Haddon, B. Knigh, Q. Li, M. Maggini, N. Martin, T. Ohno, M. Prato, T. Suzuki and F. Wudl, *Angew. Chem., Int. Ed.*, 1995, **34**, 1591–1594.
52 T. Ohno, N. Martin, B. Knigh, F. Wudl, T. Suzuki and H. Yu, *J. Org. Chem.*, 1996, **61**, 1306–1309.
53 J. W. Ryan and Y. Matsuo, *Sci. Rep.*, 2015, **5**, 1–5.
54 C. Park, H. J. Song and H. C. Choi, *Chem. Commun.*, 2009, 4803–4805.
55 F. T. Edelmann, *Angew. Chem., Int. Ed.*, 1999, **38**, 1381–1387.
56 N. Martin, *Chem. Commun.*, 2006, 2093–2104.
57 E.-Y. Zhang and C.-R. Wang, *Curr. Opin. Colloid Interface Sci.*, 2009, **14**, 148–156.
58 N. Zhou, F. Erika, S. Merschrod and Y. Zhao, *J. Am. Chem. Soc.*, 2005, **127**, 14154–14155.
59 T. Nakanishi, K. Ariga, T. Michinobu, K. Yoshida, H. Takahashi, T. Teranishi, H. Mohwald and D. G. Kurth, *Small*, 2007, **3**, 2019–2023.